Cell integrated multi-junction thermocouple array for Solid Oxide Fuel Cell temperature sensing: N+1 architecture

Journal of Power Sources 315 (2016) 70–78

Contents lists available at ScienceDirect

Journal of Power Sources

journal homepage: www.elsevier.com/locate/jpowsour

Cell integrated multi-junction thermocouple array for solid oxide fuel cell temperature sensing: N+1 architecture

Manoj Ranaweera, Jung-Sik Kim*

Aeronautical & Automotive Engineering Department, Loughborough University, LE11 3TU, United Kingdom

HIGHLIGHTS

- A multi-junction thermocouple that shares a thermo-element between junctions.
- Fabrication of multi-junction thermocouples on the cathode of SOFC.
- Performance comparison with a conventional thermocouple and discussion.
- Surface temperature measurement under thermal cycling.

ARTICLE INFO

Article history:
Received 30 September 2015
Received in revised form
4 February 2016
Accepted 2 March 2016

Keywords:
Solid oxide fuel cells
Thin-film thermocouples
Temperature sensing
SOFC degradation

ABSTRACT

Understanding the cell temperature distribution of solid oxide fuel cell (SOFC) stacks during normal operation has multifaceted advantages in performance and degradation studies. Present efforts on measuring temperature from operating SOFCs measure only the gas channel temperature and do not reveal the cell level temperature distribution, which is more important for understanding a cell's performance and its temperature-related degradation. The authors propose a cell-integrated, multi-junction thermocouple array for *in-situ* cell surface temperature monitoring of an operational SOFC. The proposed thermocouple array requires far fewer numbers of thermoelements than that required by sets of thermocouples for the same number of temperature sensing points. Hence, the proposed array causes lower disturbance to cell performance than thermocouples. The thermoelement array was sputter deposited on the cathode of a commercial SOFC using alumel (Ni:Al:Mn:Si – 95:2:2:1 by wt.) and chromel (Ni:Cr – 90:10 by wt.). The thermocouple array was tested in a furnace over the entire operating temperature range of a typical SOFC. The individual sensing points of the array were shown to measure temperature independently from each other with equivalent accuracy to a thermocouple. Thus, the concept of multi-junction thermocouples is experimentally validated and its stability on a porous SOFC cathode is confirmed.

1. Introduction

Understanding the role of operating temperature of an SOFC stack during its operation is crucial to advance the SOFC technology to a level that will deliver an economically viable solution to the future energy era. Present-day stacks are experiencing a significant level of performance deterioration and hence, not satisfactorily meeting the required life expectancy of 40,000 operating hours whilst maintaining satisfactory performance (limiting degradation to less than 10% approx.). Among various factors, thermal cycling at high temperatures (usually in a range from 600 °C to 900 °C) and uneven temperature distribution are two dominant factors that aggravate the performance deterioration. Severe mechanical failures such as formation and propagation of cracks [1] and failures in gas sealing [2] are typical temperature driven failures at cell level. A study by Blum et al. [3] showed that the problems of uneven temperature distribution extend beyond the cell level into stack level causing failures at interconnect sealing as well. However, despite the aforementioned adverse effects of the operating temperature on an SOFC's performance, some of the meritorious characteristics of SOFCs such as fuel flexibility, high energy conversion efficiency, and liberation from the expensive platinum catalyst at anode are inherited from the high operating temperature. This intricate relationship of temperature with performance

* Corresponding author.
E-mail address: j.kim@lboro.ac.uk (J.-S. Kim).

http://dx.doi.org/10.1016/j.jpowsour.2016.03.002

and degradation has necessitated the investigation of the role of temperature in performance and degradation to mitigate premature degradation of SOFC while preserving its meritorious characteristics. A comprehensive knowledge on the cell level and stack level (the whole planer area of a stack) temperature distribution of an operating SOFC is central to the success of such investigations.

Present efforts on understanding the temperature distribution over cells and stack are predominantly based on simulations, in which application of physical modelling [4–12], as well as data-driven modelling, such as artificial neural networks (ANN) [13–16], are prominent. Physical models rely on a variety of assumptions and simplifications of operating conditions, which may not realistically exist in an operating stack. Hence, experimental validations are essential to enhance the reliability of such simulations in predicting temperature distributions. In contrast, since data-driven models map input data onto output data without paying any insight into a cell's operation, they do not require a computational model of the cell operation. Thus, ANN models are free from simplifying assumptions that physical models rely on. However, the accuracy of an ANN model is governed by the accuracy of the training data set. Thus, it also requires an accurate experimental data set. Furthermore, *in situ* temperature sensing is the only possible way to investigate the detrimental evolutions of temperature profiles induced due to changes in the operating conditions such as current, flow rate, etc. [17]. Thus, experimental techniques for SOFC temperature sensing are essential.

Various experimental efforts to measure the temperature distribution within a stack are recorded in literature, though they are far more limited in number compared to simulations. Use of thermocouple thermometry, electrochemical impedance spectroscopy (EIS) [18], and Infrared (IR) thermometry [19] are the available techniques, each with their own limitations. IR imaging is an excellent technique to reveal temperature distribution over a surface with greater spatial resolution. However, the lack of visibility into inner cells of a stack does not enable it to be used in multi-cell stacks without significant stack alterations. EIS, on the other hand, is not the best suited means to reveal local temperature variations with traceable locational information. The most viable and easily adaptable technique into commercial scale stacks is the use of thermocouple thermometry. In fact, the majority of previous attempts for temperature monitoring are based on thermocouple thermometry.

Razbani et al. [14,20] embedded 5 K-type thermocouples (ϕ 0.5 mm) into the middle of a 5-cell (110 mm $\times$ 86 mm) short stack to measure temperatures from 4 corners and from the middle of a cell. Further, they state that researchers at Jülich GmbH were able to measure the temperature profile of a 5 kW SOFC stack by embedding 36 thermocouples into the stack. Guan et al. [21] and Bedogni et al. [22] have also used thermocouples to measure gas flow temperatures at the inlet and at the outlet of a stack. Although these approaches could yield successful results within their respective scopes, the inability to get temperature closer to reaction cites on a cell is a significant drawback. Nevertheless, all these research efforts have proven the suitability of thermocouple thermometry for SOFC temperature sensing. Therefore, the authors have devised to use cell-integrated thin-film thermocouples (TFTC) to get better exposure into cell level temperature distribution.

TFTC finds a number of applications in a broad application domain [23–32]. The high responsiveness, as high as 10 nS [33], is an added advantage of TFTCs. Most of the investigated applications of TFTC require temperature measurements taken from only a single point, or a few points. However, SOFCs require temperature measurements with greater spatial resolution because, there can be a significant variation of temperature across a cell [34]. Since each sensing point of a thermocouple is formed by intersection of two thermoelements, measuring temperature from SOFC with greater spatial resolution requires deposition of a large number of thermoelements on the electrodes. This is likely to cover a large portion of the effective cell area, potentially causing adverse effects to cell performance. To circumvent this problem while preserving the merits of TFTC, the authors investigated the possibility of sharing thermoelements between junctions to make multi-junction thermocouples that reduce the number of thermoelements required in multi-point temperature sensing. This paper discusses the fabrication, testing, and results of these multi-junction thermocouples fabricated on SOFC electrodes.

2. Experimental

From among different high temperature thermocouple materials, the K-type materials (alumel–Ni:Al:Mn:Si 95:2:2:1 by wt. and chromel – Ni:Cr 90:10 by wt.) were chosen for thermoelements. These materials have NIST[1] standardised performance up to 1372 °C. The external lead wires, which connect thermoelements to the data logger, were chosen from the same material as the respective thermoelements. This was to prevent formation of an intermediate junction with a third material, which may induce an undesirable additional electromotive force.

Sputter deposition (with Quorum QT150ES sputter coater) was used to fabricate thermoelements. Sputter deposition has already been successfully demonstrated for thin-film thermocouple fabrications [35]. Since the major constituent of alumel and chromel is Ni, Ni programme in the sputter coater was chosen for deposition. The preliminary research revealed that sputtering current of 150 mA and cycle time of 120 s generates the highest per-cycle film thickness. 16 cycles of sputter deposition was chosen to produce films with thickness greater than 140 nm.

The cathode was chosen as the substrate to deposit multi-junction thermocouple array to avoid any potential detrimental interactions between fuel and thermoelement materials. Since anode is exposed to fuel while cathode is exposed only to air, cathode is chemically less harmful than the anode to thermoelements. Further, cathode has a greater porosity than an un-reduced anode. That helps to investigate the survival of the array on a porous substrate. The substrate was prepared by first cleaning with acetone and then with deionised water followed by drying in a furnace at 150 °C for 10 min. This procedure expected to remove any dirt or grease on the substrate, which is likely to disturb film's adhesion to the substrate. A multi-junction thermocouple array having 4 sensing points was fabricated with 16 cycles of sputtering. Fig. 1(a) shows the fabricated array on the cathode of ϕ52 mm commercial test cell (KERAFOL®). The pattern was obtained by using two masks hand-cut from transparent binding sheets. The alumel thermoelement was deposited prior to depositing the chromel thermoelements. Width of each thermoelement is approximately 1 mm. Labels A to E represent the connection pads (3 mm $\times$ 3 mm), and S_1 to S_4 represent the 4 sensing points. The voltages measured across E-D, E-C, E-B, and E-A represent the temperatures at S_4, S_3, S_2, and S_1, respectively.

An alumel wire (ϕ0.25 mm) was connected to pad E and 4 chromel wires (ϕ0.25 mm each) were connected to pads A to D. Silver paste (from Sigma-Aldrich) was applied at each connection pad to ensure uninterrupted electrical connectivity between the wire and the film. In a case where the physical connection between a wire and a film is broken, the electrical connection was expected to be maintained through silver. Although silver acts as a foreign material at the junction when the wire and the film are not in

[1] National Institute of Standard and Technology.

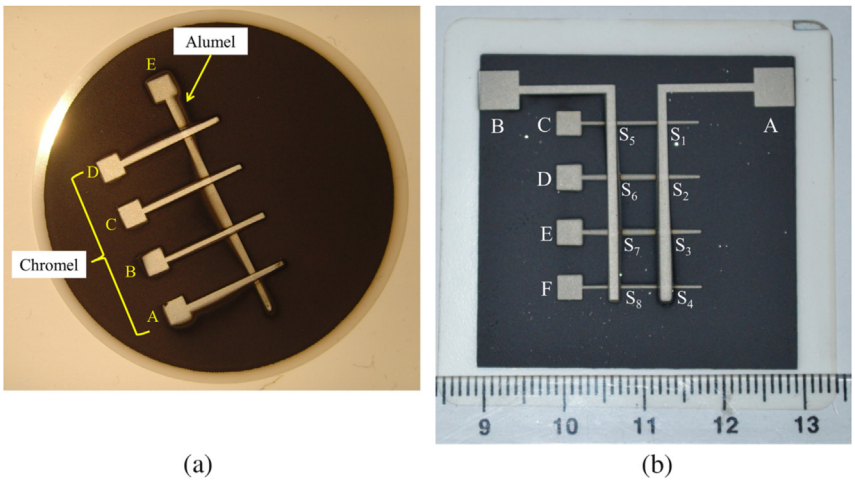

Fig. 1. (a): The single-array on ϕ52 mm electrolyte supported test cell (KERAFOL®). (b): Dual-array on the cathode (NextCell-5).

physical contact, the effect of that to temperature measurements is negligible as there cannot be a significant temperature gradient across a very tiny amount of silver within the experimental setup. Silver paste was cured at 130 °C for 40 min as per manufacturer's instructions [36]. High-pure alumina adhesive (EQ-CAA-2-LD, MTI Corporation, USA) was then applied over the connection pads to provide sufficient mechanical strength for the joint to ease handling. Since alumel and chromel form oxide layers at temperatures beyond 800 °C [37], the same alumina layer was continued over the films covering the entire length of thermoelements to prevent oxidation. Curing alumina at 250 °C for 30 min yielded a very strong layer of alumina. The lead wires were passed through ceramic beads to prevent any short circuiting during handling. Resistances across the distal ends of wires were measured before the experiment commenced; the values are given in Table 1.

The thermocouple array was placed in a box furnace while having fixed a commercial thermocouple within approximately 10 mm adjacency to the cell for dual purpose: firstly, it represents the present methods of SOFC temperature sensing by inserting thermocouples into gas channels; secondly, it is used for comparison purposes. Furnace was heated at a rate of 400 °C/hour up to 1050 °C. Once the set temperature was reached, the sensor array was rapidly cooled to introduce high level of disturbance to temperature profile. Temperatures from both thermocouple array and commercial thermocouple were recorded at 3 s intervals using NI-9213 thermocouple data logger and a specifically developed LabVIEW programme.

2.1. Dual-array thermocouple fabrication and testing

By combining two single-arrays, a dual-array was fabricated on the cathode of a 5 cm × 5 cm commercial SOFC test cell (NextCell-5), as shown in Fig. 1(b). The substrate was prepared following the same procedure as described in Section 2. The same number of sputter depositions cycles and the same sputtering parameters were used as previously to ensure similarity in film thickness between the single-array and the dual-array. The pattern was obtained by using two stainless steel masks which were not bespoke preparations for this application; hence, the widths of the two sets of thermoelements are different. The widths of thermoelements A and B on the mask is 1 mm and that of C to F is 0.2 mm on the mask. However, due to lifting of the mask under the strong magnetic field inside the sputter chamber, deposited patterns were noticeably wider than the patterns on the mask.

Thermoelements A and B are made of chromel, and elements C to F are made of alumel. External wires (ϕ0.25 mm) of the same thermoelement materials were connected as before by first using silver paste and then alumina adhesive. The entire length of thermoelements was covered with alumina adhesive as before for the same purpose. Resistances across the distal ends of the external wires were measured prior to the experiment and, the values are given in Table 2.

The dual array was placed in a box furnace while having fixed a commercial thermocouple approximately 10 mm adjacent to the cathode in the middle of it. The commercial thermocouple was again employed for a reference measurement near the cell, and for comparative purposes of evaluating the new arrangement vis-à-vis the established method. Furnace was heated to approximately 975 °C at a rate of 400 °C/hour for 4 heating-cooling cycles. Temperatures from the dual-array as well as from the commercial thermocouple were recorded at 3 s intervals. Although the array had 8 sensing points (S1 to S8), temperatures from only the first 7 points were recorded due to a limitation in the data logging system.

2.2. Results & discussion

Film thickness influences the performance of thin-film

Table 1
Resistance across external wires of single array.

External wire connection	Resistance (Ω)
A-E	20
B-E	16
C-E	13
D-E	11

Table 2
Resistances across thermoelements.

Connection pads	Corresponding sensing point	Resistance (Ω)
A-C	S_1	62
A-D	S_2	59
A-E	S_3	82
A-F	S_4	113
B-C	S_5	19
B-D	S_6	34
B-E	S_7	60
B-F	S_8	95

thermocouples [38–40]. However, the sensitivity of K-type thin-film thermocouples is independent of the film thickness when it is more than 140 nm [41]. Since the fabricated thin-films were made thicker than 140 nm, the performance can be considered unaffected by the thickness. Performance is also independent of the film width when it is greater than approximately 3 μm [42]. Therefore, the improper edge definition of fabricated films should have no effect on the performance.

The difference in resistance of 4 sensing points of the single-array (given in Table 1) is likely to be caused by the differences in the lengths of the associated thermoelements of those sensing points: the longer the thermoelement the higher the resistance. The same relationship between the length and the resistance can be seen with the dual-array as well (Table 2), however, in more noticeable magnitudes. The added resistance by the extended lengths of thermoelements in the single-array should be much lower compared to the dual-array because, the width of the single-array's thermoelements is as 5 times as higher than that of the dual-array's thermoelements. However, the exact causes of the resistance difference were not investigated as it did not appear to cause any effects on the performance. Nonetheless, aside from differences in the thermoelements' length, the substrate's (the cathode's) electrical characteristics and uneven film deposition are two plausible factors that may have introduced noticeable resistance differences.

Fig. 2 shows temperatures measured from the 4 sensing points of the single-array (S1 to S4) and from the commercial thermocouple (TC). Heating was carried out in two ways to investigate the response of multi-junction thermocouple array to different heating patters. Firstly, controlled fluctuations were introduced up to approximately 450 °C by controlling the duty-cycle. Then, steady heating was introduced. The two abrupt temperature interruptions around 680 °C and 900 °C were introduced by momentarily changing the heating power and by allowing cold air to get into the furnace chamber to investigate the nearly constant discrepancy between thermocouple's reading and the array's reading that was observed. Results show that the cell temperature measured by the single-array multi-junction thermocouple is in a very good agreement with the air temperature measured by commercial thermocouple. Further, the enlarged section of the graphs in Fig. 2 shows that the array was able to independently measure temperature from each of its sensing points via a shared common thermoelement. However, S2 demonstrated an anomalous and sudden rise in temperature beyond 1000 °C in heating, then proceeded to conform back to the pattern shown by the other sensing points when cooling down, at nearly the same temperature that it had started diverging. The experimental setup did not provide such a localised high temperature on the cell. Therefore, it should be a result of a momentary failure that had occurred somewhere between the data logger and S2 sensing point along thermoelement B.

Resistances across the distal ends of the external wires were measured after the experiment and all of those showed open circuit status. However, the cathode remained conductive having only approximately 120 Ω/cm resistance between any two points on the surface. Two plausible speculations behind this complete electrical disconnection between external wires and the thin-films are: 1) failure of thin-films 2) failure at the connection point. However, the single-array does not provide sufficient insight into distinguishing the exact failure mode. Therefore, the dual-array was fabricated and tested with an aim of investigating the cause of the electrical disconnection.

Fig. 3 shows the performance of the dual-array over 4 cycles. When NI 9213 data logger detects an open circuit in a channel, it forces the full-scale voltage across its terminals. Thus, the maximum measurable temperature of the data logger is recorded when such an open-channel is read. Therefore, the results reveal that the dual-array has lost its electrical connection to the data logger during cooling and re-gained the connection during later heating. The near-constant offset of the thermocouple array's reading with respect to the commercial thermocouple's reading during the steady heating region appeared almost alike with both the dual-array and single-array. This is an important characteristic of the results and the authors would initially like to consider two hypotheses to explain this behaviour:

1) Characteristic differences between thin-films and bulk materials

The sensor materials' Seebeck coefficients can be different between thin films and bulk material [43]. NI 9213 data logger is calibrated to work on commercial thermocouples, which uses bulk material properties. Therefore, there can be an intrinsic difference between the temperature measured from a commercial

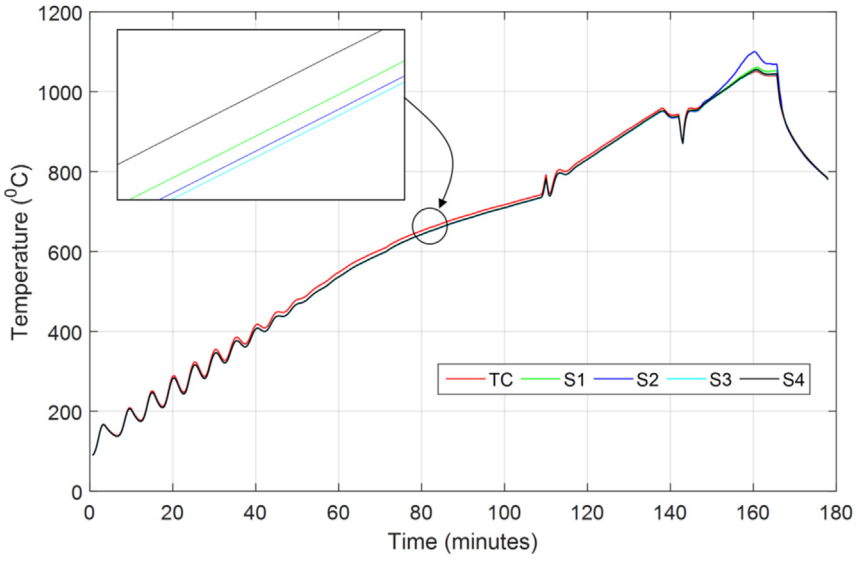

Fig. 2. Performance of thermocouple array (Legends: TC–Commercial thermocouple S1–S4: four points from array).

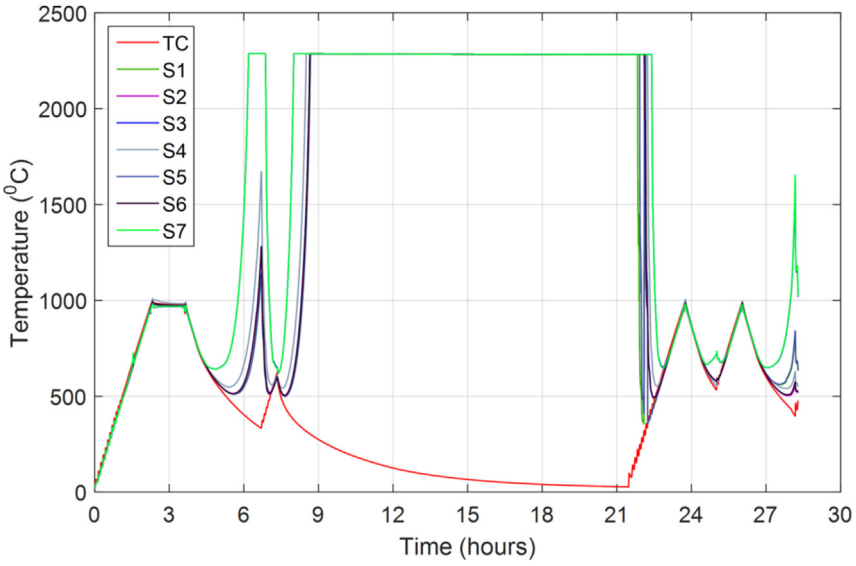

Fig. 3. Cyclic performance of dual array (TC: Commercial thermocouple, S1-S7: seven sensing points of dual array).

thermocouple and that from thin-film thermocouples, whether it is multi-junction or conventional type.

2) The effect of thermal inertia

Since the thermal inertia of SOFC test cells is higher than that of surrounding air, test cells heat up at a slower rate than the surrounding air. The temperature from commercial thermocouple is a measure of the air temperature while those from multi-junction thermocouple arrays are a measure of the cell's temperature. Therefore, the array's reading can lag behind the thermocouple's reading during heating.

Fig. 4 shows the temperature recorded during the first heating, dwelling at upper temperature limit, and cooling of the dual-array. Although the thermocouple's reading is higher during heating up process, that difference vanishes as the constant temperature region is reached. Furthermore, during cooling, the thermocouple shows faster cooling than the array. This can be a result of thermal inertia difference between the air and the substrate. Similarly, the offset of the single-array's reading from the thermocouple's reading disappears during the two temperature interruptions as seen in Fig. 2. Rapid response of the thermocouple in air, due to low thermal inertia of air, is likely to cause this disappearance of the offset. On the other hand, if the characteristic differences between thin-films and the bulk material caused the offset as suggested in the first hypothesis, the offset should be, at least, nearly linear against temperature. However, the temperature difference in the single-array, plotted against the thermocouple's temperature (Fig. 5), which is considered to be reliable enough, is highly non-linear. Therefore, after carefully considering above observations and facts, explanation of the temperature offset leans more towards the second hypothesis, namely the effect of thermal inertia.

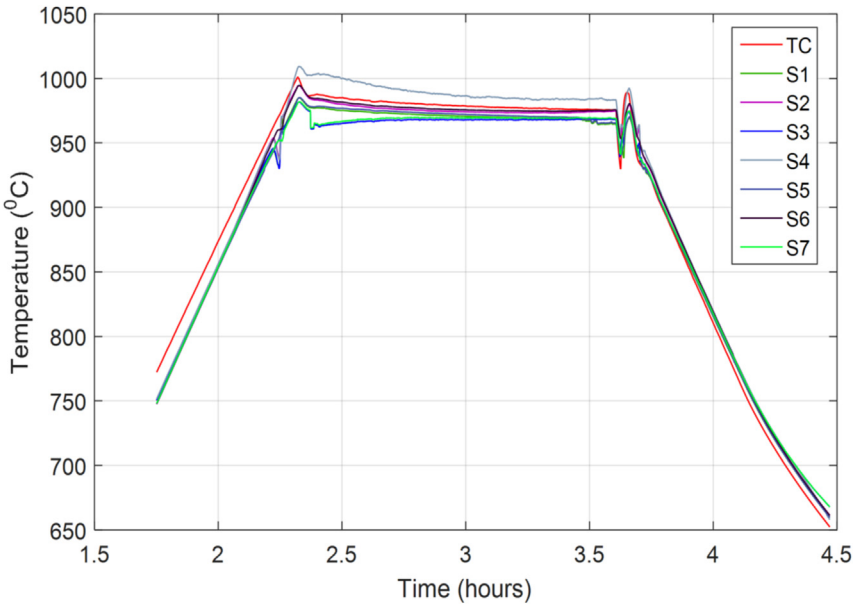

Fig. 4. First heating, dwelling, and cooling of dual-array.

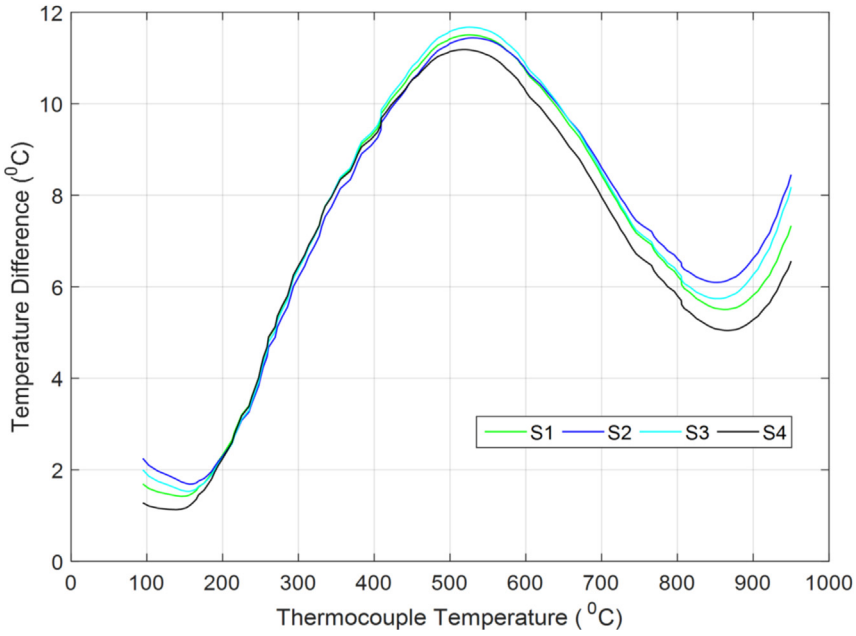

Fig. 5. Temperature difference between thermocouple and single-array (S1 – S4: 4 sensing points of single array).

Fig. 6(a) shows a momentary diversion of S3 and S7 of the dual-array from normal heating pattern encountered during the first heating cycle. The enlarged view of the encircled section, shown in Fig. 6(b), shows an almost paired behaviour of S3 and S7 during its diversion while showing an independent response prior to the incident. This signifies that the cause of failure was common to S3 and S7, even though their performance was independent from each other before the failure.

Fig. 7(a) shows the failure of the dual-array during the first cooling cycle. S3 and S7, which showed momentary diversion during heating, were the first to start failing. An enlarged view of the encircled section in Fig. 7(a) is shown in Fig. 7(b). This shows that S1/S5 and S2/S6 also failed in pairs. Furthermore, as the drift from true temperature increases, each pair converges onto a single line giving the same reading. This implies that as the cause of failure becomes more prominent, it affects the sensing points in each pair similarly.

Each pair of sensing points that failed together shared one thermoelement in common: S1/S5 pair shared thermoelement C, S2/S6 pair shared D, and S3/S7 pair shared thermoelement E (see Fig. 1(b)). The cause of failure was an electrical disconnection between thermoelements and the data logger—this is why the data logger has recorded its highest temperature at all failures. The connections at the data logger's terminals were very robust and

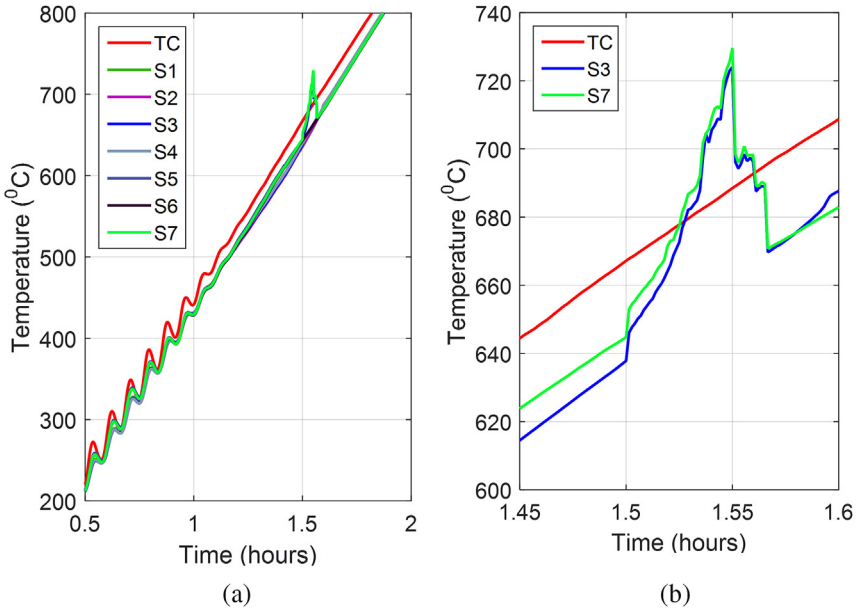

Fig. 6. (a): Momentary diversion of S3 and S7. (b) Enlarged view of the diversion.

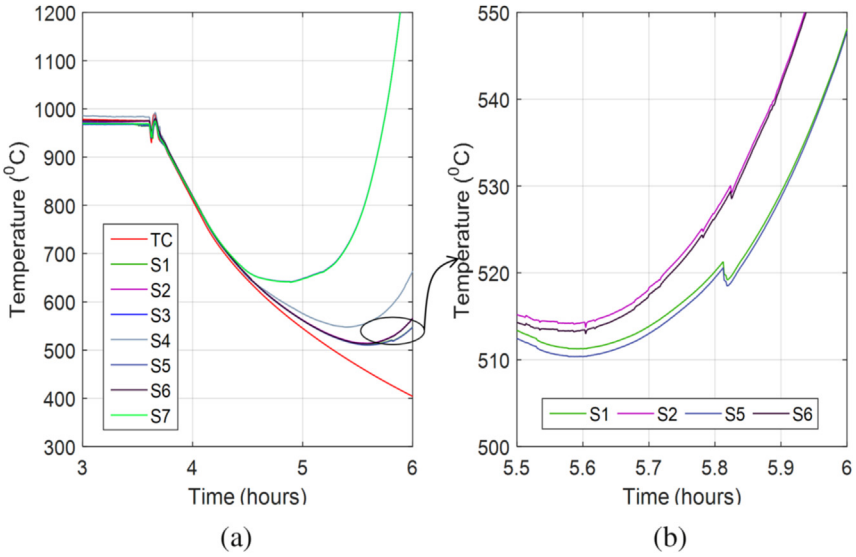

Fig. 7. (a): Failure of dual-array during first cooling. (b): Enlarged view of failure of S1, S2, S5, and S6.

they were very well maintained throughout, and even after, the experiment. Hence, the electrical disconnection has occurred either at the thin-film connection pads or on the thin-film thermoelements themselves. If thin-films failed, all failures must have occurred between a connection pad and the nearest sensing point of the corresponding pad for all thermoelements concerned. Only then does the failure become common to both sensing points on a given thermoelement and hence, the paired-like behaviour can be justified. However, there is no reason for that part of the thin-film to become significantly weaker than the rest in all 3 common thermoelements (C to E). Therefore, probability of random failure to occur within aforementioned region in all 3 thermoelements is very low. Thus, it can be speculated with high level of confidence that the failures occurred at the connection pads at C, D and E, where external wires connect to thin-film thermoelements. When a failure occurs at those connection pads, the corresponding two sensing points are affected alike. Thus, it can be well justified that the failure occurred at the connection pads. Since sensing points along thermoelement "A" or those along thermoelement "B" did not fail together, electrical connection along those two thermoelements must have been maintained well, at least, until the rest fails. Fig. 8(a) shows that the failure of dual-array occurs when the system cools below 650 °C (approx.) and it recovered when the temperature rises above that level. Furthermore, Fig. 8(b) shows that when the sensor recovered during heating, each sensing point continued to measure temperature independently from each other. Therefore, the failures at the connection pads are temperature-dependant and reversible, at least during the tested cycles. Resistance measured across the distal ends of wires after the dual-array experiment also showed complete electrical disconnection between wires and thermoelements. This is now well known to be caused by the external wire connection failure.

Stability of the external wire connection mechanism is essential to the successful application of the proposed technology into SOFC temperature sensing. The silver-based connection mechanism was used in this study only for the purpose of investigating the

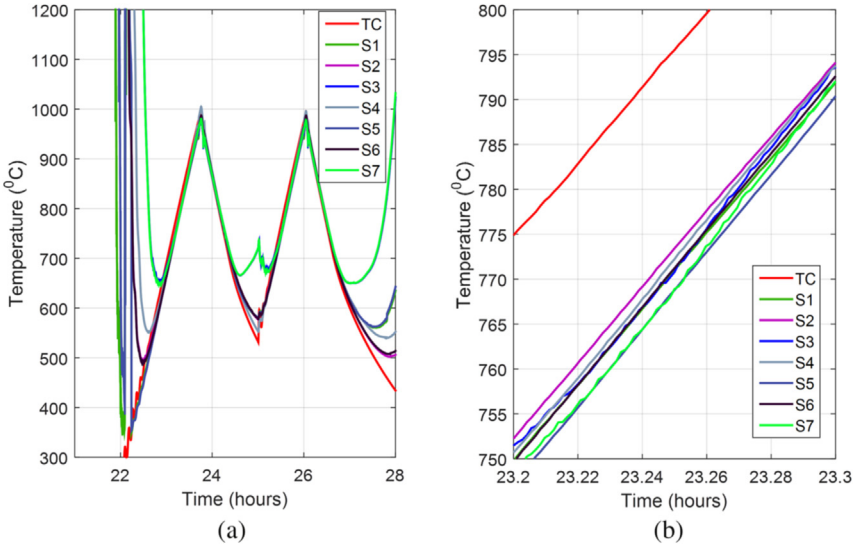

Fig. 8. (a): Failure during heating and recovery during subsequent cooling. (b): An enlarged view on a section.

feasibility of the multi-junction thermocouples. There can be a number of methods to connect external wires to thin-films where, parallel gap welding has already been successfully demonstrated in connecting external wires to thin-film thermocouples [44–46]. The authors are also investigating a mechanically loaded connection specifically focused and tailored for SOFC applications. The exact mechanism of external wire connection depends on the cell/stack geometry, space availability, as well as the required mechanical strength.

Two possible adverse effects of direct deposition of thermoelements on the cell are: (a) active cell surface masking and (b) damage to the cell or to the thermoelements themselves due to thermal stress mismatch between the cell and the thermoelements. Although one significant advantage of the proposed multi-junction thermocouple architecture over conventional thermocouples is reducing the active cell area masking, it is inventible for thermoelements to cover some part of the active cell area. However, as thermoelements can be made as narrow as approximately 3 μm [42] without affecting the temperature sensing performance, the area occupied by thermoelements is proportionally very small for most of the commercial scale SOFCs. Thus, the effect of masking is trivial in most cases. If thermal stress mismatch between the electrode and the thermoelements is found to be significant, the potential damage(s) needs to be investigated and overcome. Use of thermoelement materials, which have matching thermal expansion coefficients as the cathode, such as suitable conductive ceramics, is an option that may be adapted through further research.

3. Conclusions

The thin-film multi-junction thermocouple arrays, which were sputter deposited on cathodes of SOFC test cells, could measure cell's temperature within the entire operating temperature range of a typical SOFC (from 600 °C to 900 °C). Each sensing point could measure temperature independently from each other even when there was only a very minor temperature gradient present across junctions. Alumina-protected thin-film thermoelements could survive on the porous cathode during the entire operation. The commercial thermocouple in air, which represented the present methods of gas channel temperature measurements, responded differently to the array, particularly during temperature ramping. Therefore, the gas temperature measurements may not correctly represent a cell's temperature under temperature fluctuations. The cell integrated multi-junction thermocouple concept was proven to be successful in measuring the cell surface temperature of an SOFC with a reduced number of thermoelements.

The array could repeat measurements only beyond a certain threshold temperature (approximately 650 °C). The failure to achieve full-range repeatability was traced down to a problem with the external wire connection pads. The temporary connections made with Silver paste appear to have introduced the problems in ensuring repeatability. A robust connection mechanism needs to be adapted prior to applying the proposed multi-junction thermocouple arrays into SOFC temperature measurements.

Acknowledgement

The authors appreciate partial financial support from the India-UK Collaborative Research Initiative in Fuel Cells project on “Modelling Accelerated Ageing and Degradation of Solid Oxide Fuel Cells” (EP/I037059/1).

References

[1] H. Yokokawa, H. Tu, B. Iwanschitz, A. Mai, Fundamental mechanisms limiting solid oxide fuel cell durability, J. Power Sources 182 (2) (2008) 400–412.
[2] Y.-S. Chou, and, Stevenson, J.W, Thermal cycling and degradation mechanisms of compressive mica-based seals for solid oxide fuel cells, J. Power Sources 112 (2) (2002) 376–383.
[3] L. Blum, S.M. Groß, J. Malzbender, U. Pabst, R. Peksen, R. Peters, I.C. Vinke, Investigation of solid oxide fuel cell sealing behavior under stack relevant conditions at Forschungszentrum Jülich, J. Power Sources 196 (2011) 7175–7181.
[4] B.J. Koeppel, K. Lai, M.A. Khaleel, SOFC-MP 2D User Manual, Pacific Northwest National Laboratory, 2011.
[5] A.A. Kulikovsky, A simple equation for temperature gradient in a planar SOFC stack, Int. J. Hydrogen Energy 35 (2010) 308–312.
[6] J.D.J. VanderSteen, J.G. Pharoah, Modelling radiation heat transfer with participating media in solid oxide fuel cells, J. Fuel Cell Sci. Technol. 3 (2006) 62.
[7] E. Achenbach, Three-dimensional and time-dependent simulation of a planar solid oxide fuel cell stack, J. Power Sources 49 (1994) 333–348.
[8] H. Yakabe, T. Ogiwara, M. Hishinuma, I. Yasuda, 3-D model calculation for planar SOFC, J. Power Sources 102 (2001) 144–154.
[9] S. Nagata, A. Momma, T. Kato, Y. Kasuga, Numerical analysis of output characteristics of tubular SOFC with internal reformer, J. Power Sources 101 (2001) 60–71.
[10] K. Fischer, J.R. Seume, Thermo-mechanical stress in tubular solid oxide fuel cells: part II – operating strategy for reduced probability of fracture failure, IET Renew. Power Gener. 6 (2012) 194.
[11] M. Lockett, M.J.H. Simmons, K. Kendall, CFD to predict temperature profile for scale up of micro-tubular SOFC stacks, J. Power Sources 131 (2004) 243–246.
[12] S. Kakac, A. Pramuanjaroenkij, X.Y. Zhou, A review of numerical modeling of solid oxide fuel cells, Int. J. Hydrogen Energy 32 (2007) 761–786.
[13] D. Marra, M. Sorrentino, C. Pianese, B. Iwanschitz, A neural network estimator of Solid Oxide Fuel cell performance for on-field diagnostics and prognostics applications, J. Power Sources 241 (2013) 320–329.
[14] O. Razbani, M. Assadi, Artificial neural network model of a short stack solid oxide fuel cell based on experimental data, J. Power Sources 246 (2014) 581–586.
[15] J. Milewski, K. Swirski, Modelling the SOFC behavior by artificial neural network, Int. J. Hydrogen Energy 37 (2009) 5546–5553.
[16] J. Arriagada, P. Olausson, A. Selimovic, Artificial neural network simulator for SOFC performance prediction, J. Power Sources 112 (2002) 54–60.
[17] A. Nakajo, F. Mueller, J. Brouwer, J. Van herle, D. Favrat, Mechanical reliability and durabiulity of SOFC stacks. Part II: modelling of mechanical failure during ageing and cycling, Int. J. Hydrogen Energy 37 (2012) 9269–9286.
[18] B. Morel, R. Roberge, S. Savoie, T.W. Napporn, M. Meunier, An experimental evaluation of the temperature gradient in Solid Oxide Fuel Cells, Electrochem. Solid-State Lett. 10 (2007) B31–B33.
[19] J.E.A. Saunders, M.H. Davy, In-situ studies of gas phase composition and anode surface temperature through a model DIR-SOFC steam-methane reformer at 973.15K, Int. J. Hydrogen Energy 38 (2013) 13762–13773.
[20] O. Razbani, I. Waernhus, M. Assadi, Experimental investigation of temperature distribution over a planar solid oxide fuel cell, Appl. Energy 105 (2013) 155–160.
[21] W.B. Guan, et al., Temperature measurement and distribution inside planar SOFC stacks, Fuel Cells 12 (2012) 24–31.
[22] S. Bedogni, S. Campanari, P. Lora, L. Montelatici, P. Silva, Experimental analysis and modelling for a circular-planar type IT-SOFC, J. Power Sources 171 (2007) 617–625.
[23] J. Zhao, H. Li, H. Choi, W. Cai, J.A. Abell, X. Li, Insertable thin film thermocouples for in situ transient temperature monitoring in ultrasonic metal welding of battery tabs, J. Manuf. Process 15 (1) (2013) 136.
[24] H. Choi, X. Li, Fabrication and application of micro thin film thermocouples for transient temperature measurement in nanoseconds pulsed laser micromachining of nickel, Sensors Actuators A Phys. 136 (1) (2007) 118.
[25] G.E. Aniolek, O.J. Gregory, Thin film thermocouples for advanced ceramic gas turbine engines, Surf. Coat. Technol. 68 (1994) 70.
[26] A. Shaw, N.M. Pay, R.C. Perston, A.D. Bond, A proposed standard thermal test object for medical ultrasound, Ultrasound Med. Biol. 25 (1) (1999) 121.
[27] D. Werschmoeller, X. Li, Measurement of tool internal temperatures in the tool-chip contact region by embedded micro thin film thermocouples, J. Manuf. Process. 13 (2) (2011) 147.
[28] A. Basti, T. Obikawa, J. Shinozuka, Tools with built-in thin film thermocouple sensors for monitoring cutting temperature, Int. J. Mach. Tools Manuf. 47 (5) (2007) 793.
[29] G.K. Kreider, F. DiMeo, Platinum/Palladium thin-film thermocouples for temperature measurement on silicon wafers, Sensors Actuators A Phys. 69 (1) (1998) 46.
[30] F.R. Kennedy, D. Frusescu, J. Li, Thin film thermocouple array for sliding surface temperature measurements, Wear 207 (1–2) (2007) 46.
[31] M.S.K. Mutyala, J. Zhao, J. Li, H. Pan, C. Yuan, X. Li, In-situ temperature measurement in lithium ion battery by transferrable flexible thin film thermocouples, J. Power Sources 260 (2014) 43.
[32] J.-F. Lei, H.A. Will, Thin-film thermocouples and strain-gauge technologies for engine applications, Sensors Actuators A Phys. 65 (2–3) (1998) 187.
[33] Y. Heichal, S. Candra, E. Bordatchev, A fast-response thin film thermocouple to measure rapid surface temperature change, Exp. Therm. Fluid Sci. 33 (2) (2005) 153.

[34] E. Achenbach, Three-dimensional and time-dependent simulation of a planar solid oxide fuel cell stack, J. Power Sources 49 (1–3) (1994) 333–348.
[35] J.-F. Lei, H.A. Will, Thin-film thermocouples and strain-gauge technologies for engine applications, Sens. Actuators A Phys. 65 (2–3) (1998) 187–193.
[36] Sigma-Aldrich, Silver Conductive paste properties [online], [viewed 10/06/2015]. Available from: http://www.sigmaaldrich.com/catalog/product/aldrich/735825?lang=en&region=GB.
[37] R. Kriukience, S. Tamulevicius, High temperature oxidation of thin Chromel-Alumel thermocouples, Mater. Sci. 16 (2) (2004) 136.
[38] M. Cattani, M.C. Salvadori, A.R. Vaz, F.S. Teixeira, Thermoelectric power in very thin film thermocouples: quantum size effect, J. Appl. Phys. 100 (2006) 01.
[39] L. Yanga, Y. Zhao, C. Feng, H. Zhou, The influence of size effect on sensitivity of Cu/CuNi thin-film thermocouples, Phys. Proc. 22 (2011) 95.
[40] K.L. Chopra, S.K. Bahl, M.R. Randlett, Thermopower in thin-film copper-constantan couples, J. Appl. Phys. 39 (3) (1986) 1525.
[41] X. Zhang, H. Choi, A. Datta, X. Li, Design, fabrication and characterization of metal embedded thin film thermocouples with various film thicknesses and junction sizes, J. Micromechanics Microengineering 16 (2006) 900.
[42] H. Liu, W. Sun, Q. Chen, S. Xu, Thin-film thermocouple array for time-resolved local temperature mapping, IEEE Electron Device Lett. 32 (11) (2011) 1606–1608.
[43] W. Wunderlich, Y. Shinohara, Y. Matsumura, Magnetorn sputtering of (TiZr) NiSn thin films on different substrates for thermoelectric applications, J. Phys. Conf. Ser. 379 (2012) 01.
[44] J.-F. Lei, H.A. Will, Thin-film thermocouple and strain-gauge technologies for engine applications, Sensors Actuators A 65 (2–3) (1998) 187–193.
[45] L.C. Martin, J.D. Wrbanek, G.C. Fralick, Thin film sensors for surface measurements [in aerospace simulation facility], 19th Int. Congr. ICIASF (2001) 196–203.
[46] K.G. Kreider, D.C. Ripple, W.A. Kimes, Thin-film resistance thermometers on silicon wafers, Meas. Sci. Technol. 20 (4) (2009) 1–6.